Polarization modulation instability in a nonlinear fiber Kerr resonator

Julien Fatome[1,2,3*], Bertrand Kibler[1], François Leo[4], Abdelkrim Bendahmane[1], Gian-Luca Oppo[5], Bruno Garbin[2,3,6], Stuart G. Murdoch[2,3], Miro Erkintalo[2,3] and Stephane Coen[2,3]

[1]*Laboratoire Interdisciplinaire Carnot de Bourgogne, UMR 6303 CNRS Université Bourgogne Franche-Comté, Dijon, France.*
[2]*Department of Physics, The University of Auckland, Private Bag 92019, Auckland 1142, New Zealand.*
[3]*The Dodd-Walls Centre for Photonic and Quantum Technologies, New Zealand.*
[4]*OPERA-Photonique, Université Libre de Bruxelles, CP 194/5, 50 Av. F. D. Roosevelt, B-1050 Brussels, Belgium.*
[5]*SUPA and Department of Physics, University of Strathclyde, Glasgow G4 0NG, Scotland, EU.*
[6]*Centre de Nanosciences et de Nanotechnologies (C2N), CNRS, Université Paris-Saclay, F-91120 Palaiseau, France.*

**Corresponding author: Julien.Fatome@u-bourgogne.fr*

Received XX Month XXXX; revised XX Month, XXXX; accepted XX Month XXXX; posted XX Month XXXX (Doc. ID XXXXX); published XX Month XXXX

We report on the experimental and numerical observation of a polarization modulational instability (PMI) process occurring in a nonlinear fiber Kerr resonator. This phenomenon originates from the phase detuning between the two principal modes of polarization circulating within the cavity due to its intrinsic birefringence as well as their cross-polarization mode coupling. Our experimental investigation is based on a 10-m-long fiber ring cavity in which a polarization controller is inserted to finely control the level of birefringence imposed in the resonator. Depending on this amount of birefringence, both single-round trip (P1) and two-round trips (P2) periodic behaviors can be observed. Experimental results are well confirmed by numerical simulations based on two coupled Ikeda maps for both orthogonally polarized modes. Our study provides new insights into the control of MI in birefringent Kerr resonators and related frequency comb generation.

http://dx.doi.org/10.1364/OL.99.099999

Modulation instability (MI) is a nonlinear phenomenon occurring in Kerr media for which weak perturbations to an intense continuous-wave (cw) landscape experience an exponential growth owing to a parametric gain [1-2]. In anomalously dispersive optical fibers, MI occurs due to a perfect balance between chromatic dispersion and Kerr nonlinearity, leading to a large transfer of energy from the central cw pump into two spectral MI sidebands [1-2]. In the case of coherently-driven dissipative Kerr resonators, such as fiber ring cavities, it has been shown that the specific boundary conditions imposed on the cavity also play a crucial role in the phase matching condition leading to emergence of MI [3-5]. So far, several kinds of MI regimes and pumping configurations in fiber cavities have been reported in the literature including MI in anomalous and normal dispersion regimes, bichromatic pumping configuration, Faraday MI, incoherent pumping or period-doubled (P2) behavior [6-12]. In the temporal domain the MI process in Kerr resonators leads to the emergence of periodic patterns which are fundamentally linked to the existence of cavity solitons and related optical frequency combs in microresonators [13-16].

Less studied in coherently driven passive cavities, is the vectorial counter-part of this process, known as polarization modulational instability (PMI). Indeed, the additional degree of freedom offered by birefringence as well as the nonlinear coupling between the polarization components of light can also fulfill phase-matching conditions thus enabling the manifestation of PMI and emergence of vectorial temporal patterns [17-22].

In the present contribution, we report on the experimental observation of a polarization modulation instability process occurring in a fiber Kerr resonator. Our experimental test-bed is based on a 10-m long normally dispersive spun-fiber ring cavity including a polarization controller that enables the careful adjustment of its birefringence. This induced-birefringence impacts on the relative phase detuning between the two orthogonal polarization modes of the cavity which in turn imposes the frequency of the PMI sidebands. Moreover, we found that this amount of phase detuning can lead to single-round trip behavior (P1) or period-doubled dynamics occurring on a two-round trip cycle (P2). Experimental results are in good agreement with theoretical predictions and numerical simulations based on an iterative resolution of coupled Ikeda maps.

The experimental setup is displayed in Fig. 1(a). It consists of a passive fiber ring cavity made of a close loop of L = 10-m long normally dispersive spun fiber. The fiber is characterized by a chromatic dispersion parameter D = −44 ps/nm/km and a nonlinear Kerr parameter γ = 6.5 /W/km. It is important to notice that the fiber was specifically designed to reduce the residual birefringence by means of a fast spinning of the preform imposed during the drawing stage of the manufacturing process (spatial period of 5 mm). With such a process, any residual geometrical defect or anisotropy can be canceled out such that the fiber segment can be considered as an isotropic-like fiber ring. Furthermore, in order to prevent any additional source of residual birefringence, the fiber was carefully off-spooled and wound directly on our experimental board with a diameter close to 50 cm. Consequently, the birefringence induced by fiber-bending was estimated to be below Δn<10^{-8} [23], and can thus be neglected in our experiments.

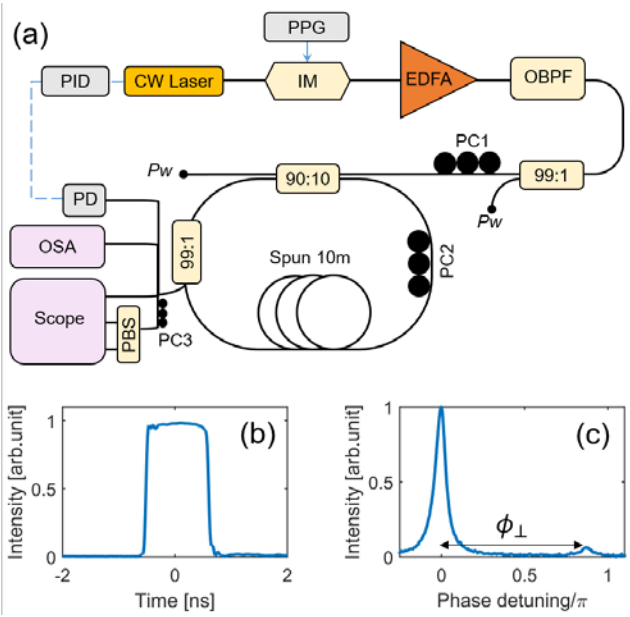

Fig. 1. (a) Experimental setup. PPG: pulse pattern generator, IM: intensity modulator, PC: polarization controller, EDFA: Erbium doped fiber amplifier, OBPF: optical bandpass filter, PBS: Polarization beam splitter, OSA: optical spectrum analyzer, PID: proportional integral derivative system, PD: photodetector, Pw: power-meter. (b) Input pulse profile. (c) Linear resonance of the cavity.

Our fiber cavity is pumped with a continuous wave (CW) laser centered at 1552.4 nm (linewidth <1 kHz), intensity-modulated to generate 1.1-ns square pulses, see Fig. 1(b), at a repetition rate of 17.54 MHz (free-spectral range of our cavity). This intensity modulation stage simultaneously enables the increase of pump peak power and the circumvention of Brillouin backscattering within the cavity. The pulsed pump is then amplified by means of an Erbium-doped fiber amplifier (EDFA) and injected into the cavity. At each round-trip, the coherent driving pump is superimposed to the circulating signal thanks to a 10:90 coupler (θ = 0.1) made of standard single mode fiber (SMF). A 99:1 SMF tap-coupler is also added to extract a part of the intra-cavity field. In this configuration, the cavity finesse was measured to be about F=27. The linear detuning seen by the pump wave at each round-trip (ϕ_0) is stabilized thanks to a proportional integral derivative (PID) system that finely adjusts the laser wavelength with respect to the nonlinear cavity resonance. At the output of the cavity, temporal, polarization and spectral characterizations of PMI are provided by means of an optical spectrum analyzer (OSA) and a real-time 50-GHz bandwidth oscilloscope coupled to a polarization beam splitter (PBS) and two fast photodetectors. Polarization management of this experiment is achieved by means of three polarization controllers (PC). First, a careful control of the input polarization state is ensured via PC1 in order to excite predominately one of the principal states of polarization (SOP) of the fiber ring. A second inner polarization controller (PC2) is implemented directly onto the spun fiber so as to finely control the level of birefringence of the cavity through mechanical stress. In this way, the phase detuning between both principal SOPs of the cavity $\phi_\perp$ can be carefully adjusted between $-\pi$ and π and can be directly monitored from measurement of both linear resonance polarization contributions, see Fig. 1(c). Finally, a third polarization controller (PC3), inserted at the output of the system enables us to select the orthogonal polarization basis for spectral and temporal characterizations.

The modelling of our vectorial Kerr resonator is based on the integration of the following coupled Ikeda maps for which u and v correspond to the right- and left-handed circular polarization components of the intracavity field at the n^{th} round-trip. Since the fiber is supposed quasi-isotropic, this map is constructed by first describing the evolution of the field envelope over one round-trip thanks to the usual system of two coupled nonlinear Schrödinger equations expressed in the circular basis: Eqs. (1). Subsequently, the boundary conditions of our resonator, Eqs. (2), are expressed in the linear polarization basis through the classical relations $E_x = (u+v)/\sqrt{2}$ and $E_y = -i(u-v)/\sqrt{2}$. These boundary conditions introduce the coherent driving and are responsible for a coherent linear mode coupling between u and v at each round-trip.

$$\begin{cases} i\frac{\partial u}{\partial z} = \frac{\beta_2}{2}\frac{\partial^2 u}{\partial t^2} - \gamma'(|u|^2 + 2|v|^2)u \\ i\frac{\partial v}{\partial z} = \frac{\beta_2}{2}\frac{\partial^2 v}{\partial t^2} - \gamma'(|v|^2 + 2|u|^2)v \end{cases} \quad (1)$$

$$\begin{cases} E_x^{n+1}(0,t) = (1-\alpha)E_x^n(L,t)e^{-i\phi_0} + \sqrt{\theta(1-\varepsilon)}E_x^{in} \\ E_y^{n+1}(0,t) = (1-\alpha)E_y^n(L,t)e^{-i(\phi_0+\phi_\perp)} + \sqrt{\theta\varepsilon}E_x^{in} \end{cases} \quad (2)$$

Here, z represents the propagation distance within the cavity and t the time in a delayed reference frame. β_2 is the second-order chromatic dispersion coefficient and γ'=2/3γ. $\alpha = \pi/F = 0.11$ represents half of the total loss of the cavity, while ϕ_0 is related to the normalized cavity detuning coefficient $\Delta = \phi_0/\alpha$. As mentioned above, $\phi_\perp$ denotes the phase birefringence and represents the phase-shift difference accumulated over one round-trip between the principal SOPs of the cavity. Finally, for the sake of simplicity, we suppose a linear polarization external pumping with a finite extinction ratio ε, meaning that both circular components are evenly excited at the input of the cavity and refer to a normalized pump power X defined as $X = \gamma L\theta P_{in}/\alpha^3$ with $P_{in} = |E_x^{in}|^2$.

In order to highlight the key role of the intra-cavity birefringence in the PMI process, we have first numerically solved the vectorial Ikeda maps described above and depicted the resulting intra-cavity spectrum with respect to the birefringence detuning $\phi_\perp$. Results are averaged over 100 realizations for a pump power X=28, a linear detuning Δ= 8, as well as a finite polarization extinction-ratio between both linear components of the pump wave ε=10^{-3} to be as close as possible to the experimental configuration. From Fig. 2(a), we see the appearance of intra-cavity modulational instability with

the generation of several harmonic frequencies around the pump wavelength. We can notice that the typical "umbrella-shape" of this map appears periodical for detuning values of $\phi_\perp$ modulo $k\pi$ and that no PMI was observed for birefringence detuning between $-0.8\pi < \phi_\perp < 0$ and $0.8\pi < \phi_\perp < \pi$. We attribute this effect by the fact that the gain of the PMI process is here not sufficient to compensate for the cavity losses. We also note that for $\phi_\perp$ very close to 0, no PMI was observed too. For these specific values, the resonator is then ruled by the isotropic PMI and requires a perfect control of the system symmetry, in particular ε=0, which is not the case in our experiments [18, 24]. For other values of $\phi_\perp$, the optimum frequency of the PMI process is found to dramatically depend on the phase detuning between both principal SOPs of the cavity. This frequency Ω_{opt} can be approximated by the following phase-matching condition, represented with circles in Fig. 2(a) and taking into account for the balance between chromatic dispersion, linear detuning, birefringence and intra-cavity power (P):

$$\Omega_{opt}^2 \frac{\beta_2 L}{2} - (mod(\phi_\perp, \pi) + \phi_0) + \gamma' PL = 0 \quad (3)$$

Note that, for $\phi_\perp$ close to zero 0, such a phase-matching condition corresponds the isotropic PMI predicted in ref. [18]. Moreover, since $(\gamma' PL - \phi_0)$ is relatively small enough in Eq. (3), the optimum PMI frequency can be well approximated by the following linear phase-matching condition:

$$\Omega_{\mathrm{opt}} = \sqrt{\frac{2mod(\phi_\perp, \pi)}{\beta_2 L}} \quad (4)$$

Fig. 2(b) depicts the corresponding concatenated experimental spectra recorded at the output of the cavity as a function of the intra-cavity birefringence $\phi_\perp$, here adjusted by means of the inner polarization controller (PC2). The input pump peak power is estimated to be X=28 (10 W) while the linear detuning is kept constant to Δ=8. We can observe a good qualitative agreement with our previous numerical simulations of Fig. 2(a) and in particular the typical "umbrella-shape" mapping of this process characterized by the emergence of well separated, far detuned and thin sidebands corresponding to PMI frequencies. We can also notice the appearance of an additional parametric gain occurring around $\Omega_{\mathrm{opt}}/2$ both in numerical and experimental spectra which corresponds to a vectorial four-wave mixing process between the linearly polarized pump wave and the first orthogonal sideband.

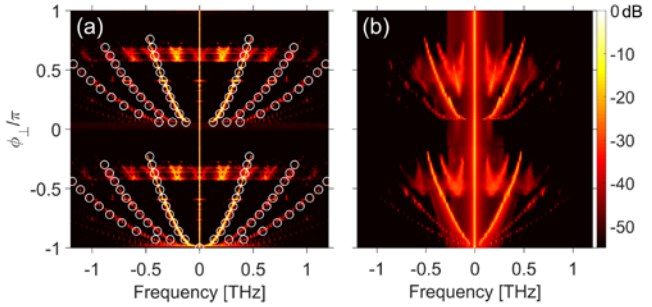

Fig. 2. Pseudo-color plots reporting the evolution of the output spectrum according to the birefringence detuning $\phi_\perp$. (a) Numerical results are compared with theoretical predictions of Eq. (3) in circles. (b) Corresponding experimental results. In both cases, the input power was estimated to X=28 and the linear detuning is kept constant to Δ=8. Data values are normalized with respect to the pump power.

To summarize and fairly compare the different results obtained from numerical simulations, experiments and theoretical predictions, we have reported in Fig. 3(a) the frequencies of the first-order PMI sidebands as a function of the birefringence detuning $\phi_\perp$. We can observe a good agreement between our measurements (circles), numerical results (stars) and phase-matching condition (dashed-line).

In order to further assess the vectorial nature of the observed PMI process, we have recorded the output spectrum projected along the orthogonal polarization basis corresponding to the pump SOP and its orthogonal component. The results are reported in Fig. 3(b) for a birefringence detuning $\phi_\perp$=0.2π. They clearly show that the first MI sidebands are mainly generated orthogonally to the pump wave with an extinction-ratio above 20 dB and then alternate between both SOPs for the higher-order sidebands. This behavior is similar to the general case observed in conventional isotropic PMI experiments performed in single-pass fiber segments [25].

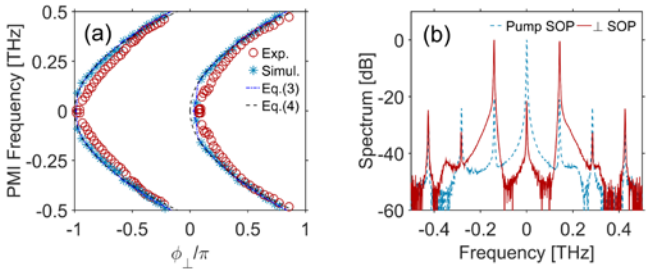

Fig. 3. (a) Optimum PMI frequency (Ω_{opt}) for the first-order sideband as a function of the birefringence detuning $\phi_\perp$. Experimental results (red circles) are compared with numerical simulations (blue stars) as well as theoretical predictions of Eqs. (3) and (4) (blue and black dashed-lines). (b) Output spectrum for $\phi_\perp$=0.2π recorded behind the output PBS and decomposed into the orthogonal basis corresponding to the pump SOP and its orthogonal component.

In addition to the spectral analysis shown in Figs. 2 and 3, we have also performed a temporal characterization of the intra-cavity intensity profile thanks to a 50-GHz bandwidth real-time oscilloscope. To this aim, by adjusting the inner polarization controller PC3, the birefringence of the cavity $\phi_\perp$ was finely adjusted close to 0 so as to generate a periodic MI pattern within the bandwidth of our 50-GHz photodetectors.

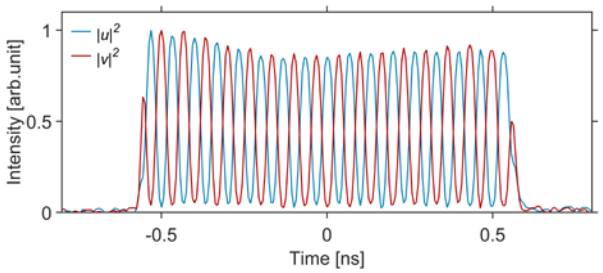

Fig. 4. Typical experimental intensity profiles of both orthogonal components monitored at the output of the cavity obtained for $\phi_\perp$~0.

We have then monitored the corresponding temporal profile at the output of the PBS. The output polarization basis was carefully adjusted in such a way to maximize the contrast of the oscillations between both orthogonal polarization components. Note that from a theoretical point of view, this basis is supposed to be the right- and left- circular components of the intra-cavity field ($|u|^2$ and $|v|^2$). In

practice, however, the principal SOPs of the cavity are doubtless elliptical instead of perfectly linear and thus the output polarization basis remains arbitrary selected. Figure 4 illustrates the typical experimental intensity profiles of this PMI phenomenon. We can observe large temporal oscillations at a repetition rate of 15 GHz as well as a perfect anti-correlation between both polarization components, as expected from vectorial MI process [17, 18, 25].

The temporal evolution of the PMI process is even more interesting when monitored as a function of circulating round-trips. To this aim, single-shot data sequences recorded on a long temporal window have been acquired on our oscilloscope so as to reconstruct the evolution of the intra-cavity field from round-trip to round-trip. Figure 5(a) displays the evolution (from bottom to top) of the polarization component ($|u|^2$) recorded for $\phi_\perp \gtrsim 0$. We can observe a steady-state evolution with a constant periodic MI pattern recirculating into the cavity with one round-trip period (P1 behavior). Note here the typical polarization nature of this PMI process for which the total intensity profile, shown in Fig. 5(b), remains perfectly constant along the propagation. The modulated pattern is only visible in the polarization domain. Figures 5(c) and 5(d) display the results obtained for a birefringence detuning close to $-\pi$. In this case, as can be seen in the checkerboard-like mapping of Fig. 5(c), the anti-resonant phase matching condition leads to a period-doubled P2 behavior for which the PMI pattern switches between the two polarization components at each round-trip [19]. This behavior is another consequence of the linear mode coupling induced by the residual birefringence at each round-trip. Indeed, for a specific value of $\phi_\perp \sim \pm\pi$, the fiber ring then acts as a half-wave-plate. Therefore, this half-wave-plate process swaps the light's handedness at each round-trip, and gives rise to the flipping of the PMI pattern on a two-round-trips period [26]. Finally, note that similarly to the previous case, the total intensity profile in Fig. 5(d) remains constant, thus concealing the polarization information.

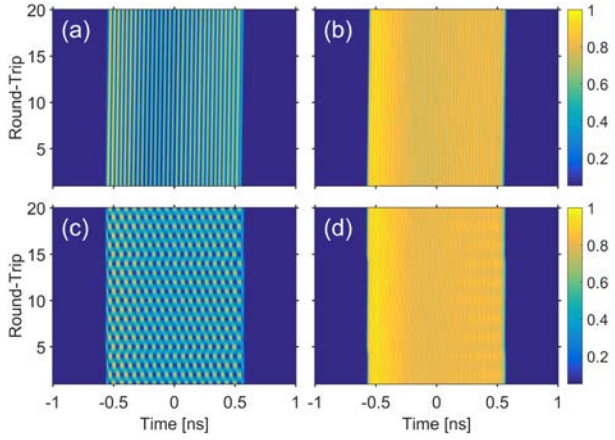

Fig. 5. (a) Experimental evolution (from bottom to top) of the intensity profile monitored on the polarization component $|u|^2$ as a function of round-trips for $\phi_\perp \sim 0$ (b) Corresponding total intensity profile (before PBS). (c & d) Same as (a& b) but with $\phi_\perp$ dose to $-\pi$.

In conclusion, we have reported the experimental observation of polarization modulational instability in a fiber Kerr resonator. It was shown that the phase matched PMI frequency is directly related to the level of the intrinsic birefringence present in the resonator and can be well approximated through a phase-matching condition taking into account for this polarization phase detuning. Our experimental observations were performed thanks to a 10-m long spun fiber ring cavity for which an inner polarization controller enables us to accurately control the level of birefringence. By means of real-time temporal characterizations, both single-round trip (P1) and period-doubled (P2) behaviors have been highlighted. Experimental results were found to be in good agreement with theoretical predictions and numerical simulations based on coupled Ikeda maps. Finally, these results provide new insights into the allowing control of dissipative MI in birefringent nonlinear resonators as well as a potential new degree of freedom for frequency comb generation in normal dispersion Kerr resonators by exploiting linear mode coupling.

Funding. J. F. acknowledges the financial support from the Conseil Régional de Bourgogne Franche-Comté, APEX project and International Mobility Program as well as FEDER, Optiflex project. B. K. acknowledges support from the ANR (Project No. PIA2/ISITE-BFC, contract n° ANR-15-IDEX-03).

Disclosures. The authors declare no conflicts of interest.

References

1. K. Tai, A. Hasegawa, and A. Tomita, Phys. Rev. Lett. **56**, 135 (1986)
2. G. P. Agrawal, *Nonlinear Fiber Optics* (5th ed., Academic Press, Oxford, 2013).
3. M. Nakazawa, K. Suzuki, and H. A. Haus, Phys. Rev. A **38**, 5193 (1988).
4. R. Vallée, Opt. Commun. **81**, 419 (1991).
5. M. Haeltermann, S. Trillo, and S. Wabnitz, Opt. Commun. **91**, 401 (1992).
6. S. Coen and M. Haelterman, Phys. Rev. Lett. **79**, 4139 (1997).
7. F. Copie, M. Conforti, A. Kudlinski, A. Mussot, and S. Trillo, Phys. Rev. Lett. **116**, 143901 (2016).
8. D. Ceoldo, A. Bendahmane, J. Fatome, G. Millot, T. Hansson, D. Modotto, S. Wabnitz, and B. Kibler, Opt. Lett. **41**, 5462 (2016).
9. M. Conforti, A. Mussot, J. Fatome, A. Picozzi, S. Pitois, C. Finot, M. Haelterman, B. Kibler, C. Michel, and G. Millot, Phys. Rev. A **91**, 023823 (2015).
10. A. Bendahmane, J. Fatome, C. Finot, G. Millot, and B. Kibler, Opt. Lett. **42**, 251 (2017).
11. T. Hansson and S. Wabnitz, J. Opt. Soc. Am. B **32**, 1259 (2015).
12. F. Bessin, F. Copie, M. Conforti, A. Kudlinski, A. Mussot, and S. Trillo, Phys. Rev. X **9**, 041030 (2019).
13. S. Coen and M. Haelterman, Opt. Lett. **26**, 39 (2001).
14. F. Leo, S. Coen, P. Kockaert, S. P. Gorza, P. Emplit, and M. Haelterman, Nat. Photon. 4, 471-476 (2010).
15. A. A. Savchenkov, A. B. Matsko, and L. Maleki, Nanophoton. **5**, 363 (2016).
16. P. Del'Haye, A. Schliesser, O. Arcizet, T. Wilken, R. Holzwarth, and T. J. Kippenberg, Nature **450**, 1214 (2007).
17. A. L. Berkhoer, and V. E. Zakharov, Sov. Phys. JETP **31**, 486 (1970).
18. M. Haelterman, S. Trillo, and S. Wabnitz, JOSA B **11**, 446 (1994).
19. M. Haelterman and M. D. Tolley, Opt. Commun. **108**, 167 (1994).
20. I. P. Areshev, T. A. Murina, N. N. Rosanov and V. K. Subashiev, Opt. Commun. **47**, 414 (1983).
21. A. Tonello, Opt. Quant. Electron. **32**, 1219-1238 (2000).
22. T. Hansson, M. Bernard, and S. Wabnitz, J. Opt. Soc. Am. B **35**, 835 (2018).
23. L. Palmieri, A. Galtarossa, and T. Geisler, Opt. Lett. **35**, 2481 (2010).
24. B. Garbin, J. Fatome, G.-L. Oppo, M. Erkintalo, S. G. Murdoch, and S. Coen, arXiv:1904.07222, to be published in Phys. Rev. Research (2020).
25. P. Kockaert, M. Haelterman, S. Pitois, and G. Millot, Appl. Phys. Lett. **75**, 2873 (1999).
26. J. Fatome, Y. Wang, B. Garbin, B. Kibler, A. Bendahmane, N. Berti, G.-L. Oppo, F. Leo, S. G. Murdoch, M. Erkintalo and S. Coen., in Advanced Photonics Congress, paper JTu6F.2 (2018).

Full References

1. K. Tai, A. Hasegawa, and A. Tomita, Observation of modulation instability in optical fibers, Phys. Rev. Lett. **56**, 135 (1986).
2. G. P. Agrawal, Nonlinear Fiber Optics (5th ed., Academic Press, Oxford, 2013).
3. M. Nakazawa, K. Suzuki, and H. A. Haus, "Modulational instability oscillation in nonlinear dispersive ring cavity," Phys. Rev. A **38**, 5193 (1988).
4. M. Haeltermann, S. Trillo, and S. Wabnitz, "Dissipative modulation instability in a nonlinear dispersive ring cavity," Opt. Commun. **91**, 401-407 (1992).
5. S. Coen and M. Haelterman, "Modulational instability induced by cavity boundary conditions in a normally dispersive optical fiber," Phys. Rev. Lett. **79**, 4139 (1997).
6. R. Vallée, "Temporal instabilities in the output of an all-fiber ring cavity," Opt. Commun. **81**, 419-426 (1991).
7. F. Copie, M. Conforti, A. Kudlinski, A. Mussot, and S. Trillo, "Competing Turing and Faraday instabilities in longitudinally modulated passive resonators," Phys. Rev. Lett. **116**, 143901 (2016).
8. D. Ceoldo, A. Bendahmane, J. Fatome, G. Millot, T. Hansson, D. Modotto, S. Wabnitz, and B. Kibler, "Multiple four-wave mixing and Kerr combs in a bichromatically pumped nonlinear fiber ring cavity," Opt. Lett. **41**, 5462-5465 (2016).
9. M. Conforti, A. Mussot, J. Fatome, A. Picozzi, S. Pitois, C. Finot, M. Haelterman, B. Kibler, C. Michel, and G. Millot, "Turbulent dynamics of an incoherently pumped passive optical fiber cavity: Quasisolitons, dispersive waves, and extreme events," Phys. Rev. A **91**, 023823 (2015).
10. A. Bendahmane, J. Fatome, C. Finot, G. Millot, and B. Kibler, "Coherent and incoherent seeding of dissipative modulation instability in a nonlinear fiber ring cavity," Opt. Lett. **42**, 251-254 (2017).
11. T. Hansson and S. Wabnitz, "Frequency comb generation beyond the Lugiato-Lefever equation: multi-stability and super cavity solitons," J. Opt. Soc. Am. B **32**, 1259-1266 (2015).
12. F. Bessin, F. Copie, M. Conforti, A. Kudlinski, A. Mussot, and S. Trillo, "Real-Time Characterization of Period-Doubling Dynamics in Uniform and Dispersion Oscillating Fiber Ring Cavities," Phys. Rev. X **9**, 041030 (2019).
13. S. Coen and M. Haelterman, "Continuous-wave ultrahigh-repetition-rate pulse-train generation through modulational instability in a passive fiber cavity," Opt. Lett. **26**, 39-41 (2001).
14. F. Leo, S. Coen, P. Kockaert, S. P. Gorza, P. Emplit, and M. Haelterman, "Temporal cavity solitons in one-dimensional Kerr media as bits in an all-optical buffer," Nat. Photon. **4**, 471-476 (2010).
15. A. A. Savchenkov, A. B. Matsko, and L. Maleki, "On frequency combs in monolithic resonators," Nanophoton. **5**, 363-391 (2016).
16. P. Del'Haye, A. Schliesser, O. Arcizet, T. Wilken, R. Holzwarth, and T. J. Kippenberg, "Optical frequency comb generation from a monolithic microresonator," Nature **450**, 1214-1217 (2007).
17. A. L. Berkhoer, and V. E. Zakharov, "Self-excitation of waves with different polarizations in nonlinear media," Sov. Phys. JETP **31**, 486-490 (1970).
18. M. Haelterman , S. Trillo, and S. Wabnitz, "Polarization multistability and instability in a nonlinear dispersive ring cavity," JOSA B **11**, 446-456 (1994).
19. M. Haelterman and M. D. Tolley, "Pure polarization period-doubling instability in a Kerr-type nonlinear ring cavity," Opt. Commun. **108**, 167-175 (1994).
20. I. P. Areshev, T. A. Murina, N. N. Rosanov and V. K. Subashiev, "Polarization and amplitude optical multistability in a nonlinear ring cavity," Opt. Commun. **47**, 414-419 (1983).
21. A. Tonello, "The role of birefringence in modulation instability fiber ring resonators," Opt. Quant. Electron. **32**, 1219-1238 (2000).
22. T. Hansson, M. Bernard, and S. Wabnitz, "Modulational instability of nonlinear polarization mode coupling in microresonators," J. Opt. Soc. Am. B **35**, 835-841 (2018).
23. L. Palmieri, A. Galtarossa, and T. Geisler, "Distributed characterization of bending effects on the birefringence of single-mode optical fibers," Opt. Lett. **35**, 2481-2483 (2010).
24. B. Garbin, J. Fatome, G.-L. Oppo, M. Erkintalo, S. G. Murdoch, and S. Coen "Asymmetric balance in symmetry breaking," arXiv:1904.07222, to be published in Phys. Rev. Research (2020).
25. P. Kockaert, M. Haelterman, S. Pitois, and G. Millot, "Isotropic polarization modulational instability and domain walls in spun fibers," Appl. Phys. Lett. **75**, 2873-2875 (1999).
26. J. Fatome, Y. Wang, B. Garbin, B. Kibler, A. Bendahmane, N. Berti, G.-L. Oppo, F. Leo, S. G. Murdoch, M. Erkintalo, and S. Coen., "Flip-flop polarization domain walls in a Kerr resonator", in Advanced Photonics Congress, paper JTu6F.2 (2018).